ACS APPLIED MATERIALS & INTERFACES

Research Article

www.acsami.org

High-Performance Nanocomposite Based Memristor with Controlled Quantum Dots as Charge Traps

Adnan Younis,[†] Dewei Chu,*[,†] Xi Lin,[†] Jiabao Yi,[†] Feng Dang,[‡] and Sean Li[†]

[†]School of Materials Science and Engineering, University of New South Wales, Sydney, 2052, NSW, Australia

[‡]Research Center for Materials Backcasting Technology (MBT Center), Nagoya University, Nagoya 464-8603, Japan

Supporting Information

ABSTRACT: We report a novel approach to improve the resistive switching performance of semiconductor nanorod (NR) arrays, by introducing ceria (CeO_2) quantum dots (QDs) as surface charge trappers. The vertically aligned zinc oxide (ZnO) (NR) arrays were grown on transparent conductive glass by electrochemical deposition while CeO_2 QDs were prepared by a solvothermal method. Subsequently, the as-prepared CeO_2 QDs were embedded into a ZnO NR array by dip coating to obtain a CeO_2−ZnO nanocomposite. Interestingly, such a device exhibits excellent resistive switching properties with much higher ON/OFF ratios, better uniformity, and stability over the pure ZnO and CeO_2 nanostructures. The origin of resistive switching was studied and the role of heterointerface was discussed.

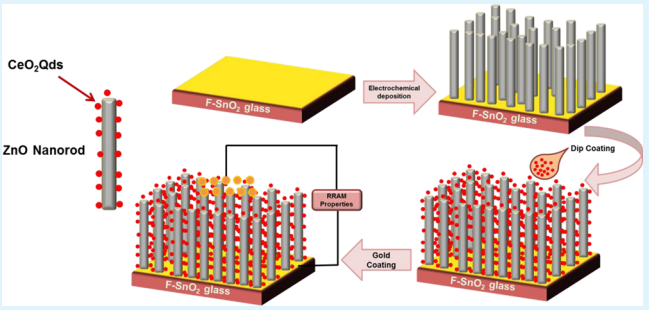

KEYWORDS: *electrochemical deposition, solvothermal process, resistive switching, quantum dots, charge traps, charge transport*

INTRODUCTION

Bottom-up nanofabrication approaches involving direct interfacing and integration of low-dimension nanostructures, especially vertically aligned one-dimensional (1D) nanorod (NR) arrays, potentially provide an attractive solution to attain ultrahigh-density advanced nanoscale devices in three-dimensional (3D) nanocircuits.[1,2] Vertically aligned semiconductor nanowire/NR arrays have been successfully utilized as building blocks for various electronic and photonic devices, including light-emitting diodes, field-effect transistors, and resistive random access memories (RRAMs, or memristors).[3−9] For instance, compared to polycrystalline films, nanoscale arrays have unique advantages in RRAM applications,[10] because the localized filamentary conducting paths in the polycrystalline films are diverse in each switching. This leads to the nonuniform distributions of switching voltages and resistance states that result in irresolvable errors in the memristor operations. Chang et al.[11] demonstrated resistive switching characteristics for vertically aligned ZnO NR layers. The distinct geometry of ZnO NRs leads to excellent nonvolatile behavior with a narrow dispersion of on/off ratio, because of the formation of straight and extensible conducting filaments along the direction of each of the vertically aligned ZnO NRs. Most recently, the resistive switching properties in vertically aligned TiO_2 nanotubes and the formation of conducting filaments along the nanotube walls were presented, to explain the switching properties.[12]

To further improve resistive switching performance, transition-metal ions have also been introduced to enlarge the memory window via increasing the resistivity of the high-resistance status. For example, Yang et al.[13] demonstrated ultrafast programming speed with high R_{OFF}/R_{ON} and greater retention time for fully room-temperature-prepared Mn-doped ZnO resistive switching memory devices. However, the solubility of transition-metal ions in ZnO is usually extremely low and doping may cause undesired structures, as well as characterization alteration. As an alternative method, the development of nanocomposites can be deployed in this context and it is expected to have advantages in the combination of both materials. As to ZnO (NRs), the principle of choosing second materials should be as follows: (1) the material also exhibits resistive switching behavior; and (2) the morphology should have the best compatibility with the ZnO NR matrix. Therefore, this type of material should be compatible because of the smaller size (e.g., quantum dots), so that it has a good connection with ZnO NRs as well as large interface interaction.

RRAM devices based on ceria (CeO_2) nanostructures has been recently reported by our group with stable bipolar resistive switching characteristics and indicated that CeO_2 is a potential material for RRAM applications.[14] It is well-known that ultrasmall CeO_2 nanoparticles with excellent redox properties contain a higher density of surface defects (e.g., oxygen vacancies), which is a function of the mixed valence states. These oxygen vacancies may lead to the generation of localized electrons on the surface of the CeO_2 nanoparticles,

Received: January 22, 2013
Accepted: March 7, 2013
Published: March 7, 2013

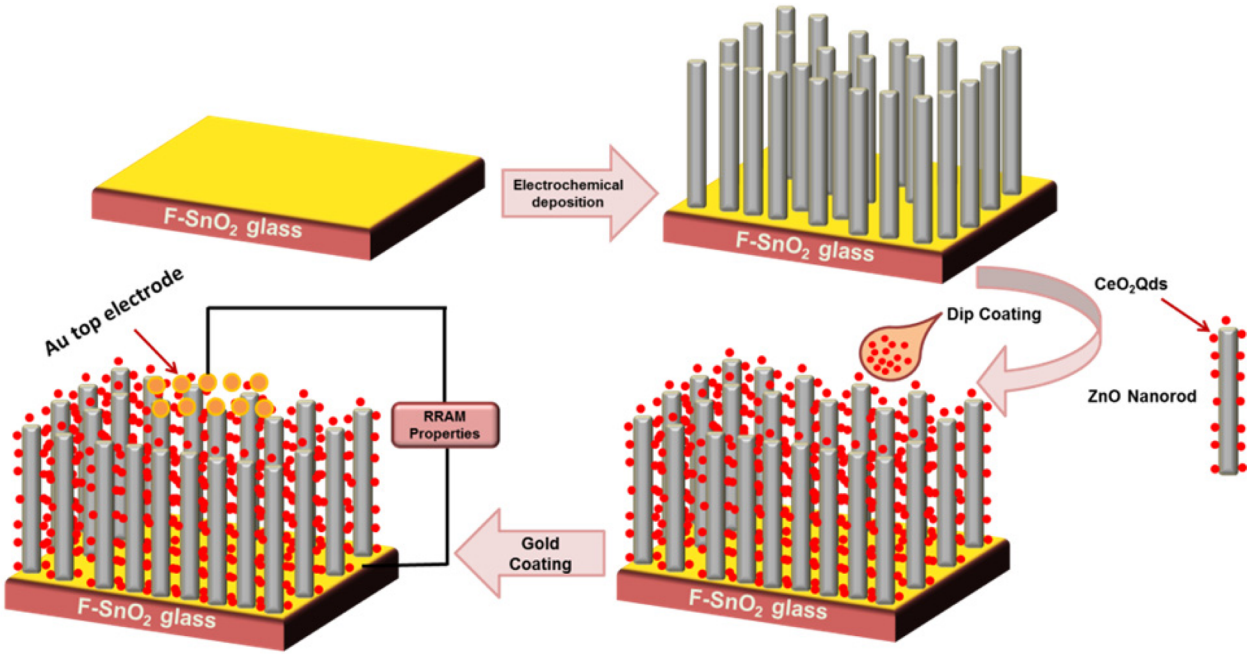

Figure 1. Schematic diagram for the growth process of a CeO_2–ZnO nanocomposite and the fabrication of a memory device.

which might play a vital role in tuning the resistive switching properties of ZnO. It is suggested that the CeO_2–ZnO heterostructures with an optimal composition and/or morphology may modulate better resistive switching properties. Therefore, it is of great interest to investigate the RS characteristics of such heterogeneous binary oxide system.

In this work, we developed ZnO NR array/CeO_2 quantum dot (QD) nanocomposites with high-performance resistive switching properties. ZnO NR arrays were grown directly on the transparent conductive fluorine tin oxide glass substrate (FTO) via a simple electrochemical deposition method. Ultrasmall (~5 nm) CeO_2 QDs were synthesized via a hydrothermal process. The nanocomposite structure composed of CeO_2–ZnO were then formed by simple layer by layer deposition of CeO_2 (QDs) on vertically aligned ZnO NRs. To the best of our knowledge, the present work is the first attempt to explore the controllable synthesis of a hierarchical CeO_2–ZnO structure. It is believed that this approach can also be used to fabricate many similar electronic devices with high performance and long durability.

EXPERIMENTAL SECTION

Synthesis. All chemicals were purchased from Sigma–Aldrich and without further purification. First, a ZnO NRs array was deposited electrochemically on FTO glass (9.3–9.7 Ω, Asahi Glass Corporation, Japan, 1.1 mm × 26 mm × 30 mm). The detailed procedure for the synthesis of ZnO NRs was presented elsewhere.[15] In the second step, CeO_2 QDs were prepared using a solvothermal process. In the typical synthesis process, 15 mL of a 16.7 mmol/L cerium(III)nitrate aqueous solution was added into a 50-mL autoclave, and then a 15-mL mixed solution of toluene, oleic acid (OLA, 0.56 mL), and *tert*-butylamine (0.15 mL) was added to the autoclave in open air without stirring. The sealed autoclave was heated at 180 °C for 72 h, and then cooled to room temperature. The upper organic crude solution was centrifuged to separate the CeO_2 nanocrystals. The separated CeO_2 QDs were redispersed into 3 mL of toluene. The molar ratio of OLA/Ce in the synthesis was 8:1.[16]

At the final stage, the redispersed CeO_2 QDs were deployed on a ZnO NR array, using a simple drop technique. This process was repeated 15 times to get the final form of the CeO_2–ZnO nanocomposite film. Small area of electrode (Au) with square patterning was coated by sputtering using a metal shadow mask. The CeO_2–ZnO film was thermally annealed at 350 °C for 15 min in an ambient atmosphere to eliminate organics. The processing procedure is schematically illustrated in Figure 1.

Characterization. The structural analysis of the fabricated CeO_2–ZnO nanocomposite was carried out using an X-ray diffraction (XRD) system (Philips X'pert Multipurpose X-ray Diffraction System (MPD) with Cu Kα radiation), whereas a scanning electron microscopy (SEM) system (Nova Nano SEM 230) was used to examine the surface morphology. Energy-dispersive spectroscopy (EDS) equipment that was attached to the SEM system was used to analyze the composition of the structure. Transmission electron microscopy (TEM) investigations were carried out by a Philips CM200 microscope. The resistive switching (RS) characteristics were measured using an Autolab 302N electrochemical workstation controlled with Nova software. The varied temperature experiments were performed in the temperature range of 290–480 K, while all the other electrical measurements were performed in air at room temperature.

RESULTS AND DISCUSSIONS

The morphologies of ZnO NRs array and CeO_2 QDs, as well as the CeO_2–ZnO nanocomposite, are shown in Figure 2. The average diameter and the length of the ZnO NRs are (~20 nm) and (~200 nm), respectively, while the average diameter of the CeO_2 QDs is (~5 nm). The irregularity in the shape of the CeO_2 QDs (see inset of Figure 2b) indicates the presence of surface defects. The CeO_2 QDs are found to be well surrounded by the ZnO NRs (see Figure 2d), hence confirming the desired morphology.

A typical XRD pattern of the CeO_2–ZnO nanocomposite, depicted in the inset of Figure 2c, shows well-defined (002) diffraction characteristic peaks for ZnO (JCPDS File Card No. 36-1451) and the (111) plane of CeO_2 (JCPDS File Card No. 34-394), respectively. The strong peak of (002) indicates the formation of vertically aligned ZnO NRs on the conducting substrate, while the presence of CeO_2 (111) characteristic peak

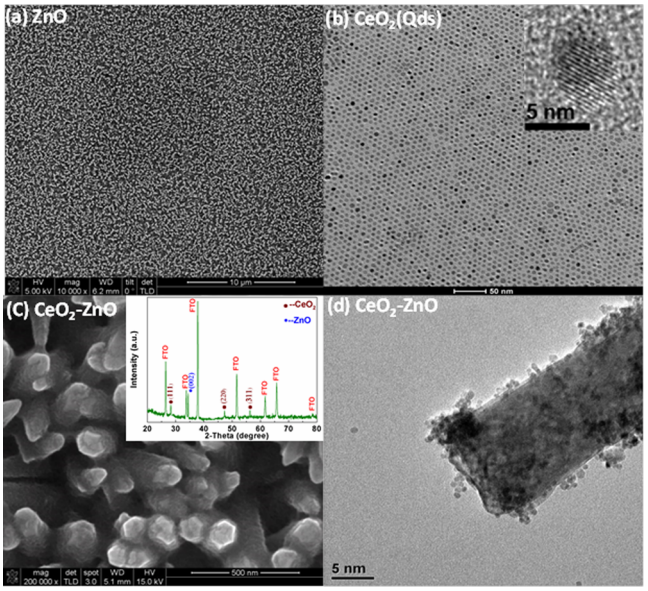

Figure 2. (a) Surface morphology of ZnO NRs. (b) TEM image of CeO_2 QDs (inset shows a high-resolution transmission electron microscopy (HRTEM) image of a single CeO_2 QD). (c) Surface morphology of a CeO_2–ZnO nanocomposite (inset shows the XRD pattern of CeO_2–ZnO). (d) TEM image of a single ZnO NR embedded with CeO_2 (QDs).

verified the appearance of CeO_2 in the nanocomposite structure.

The EDX line scanning profile of a sample cross-section (see Figure S1 in the Supporting Information) confirmed the presence of cerium along the distribution of elemental zinc in the cross-sectional image. The location and direction of the line scan is depicted by an arrow on the corresponding SEM cross-sectional image. A line scan shows that the characteristic X-ray signals of Zn and Ce rise and drop when the line scan intercepts and leaves the CeO_2–ZnO matrix and goes into the FTO glass substrate. The X-ray signal of O did not fall at the end, because of its presence in the FTO glass substrate as well.

The current–voltage (I–V) characteristics for all samples were carried out by sweeping voltage in the sequence of 0 V → −3 V → 0 V → +3 V → 0 V and at a sweeping speed of 0.01 V/s. In the first voltage sweep, a transition from the high-resistance state (HRS) to the low-resistance state (LRS) was observed at approximately −1.9 V and the device retained this state for the following sweep. The device was set back to the OFF state (HRS) at approximately +2.08 V, exhibiting the bipolar resistive switching nature of the device.

Good endurance is the fundamental challenge for nonvolatile memory devices (NVM) and electric-pulse-induced resistive switching measurements are conducted. Figure 3b shows the nondegradable endurance characteristics with 200 cycles in our CeO_2–ZnO nanocomposite device.

To demonstrate the stability of the resistive switching properties in the CeO_2–ZnO nanocomposite device, data retention was gauged by examining the current level of the device in the ON state over a long period of time (>10^4 s) at room temperature (Figure 3c). A well-maintained resistance ratio (HRS:LRS) was observed in the device with narrow scattering for more than 10^4 s.

In order to further understand the performance of CeO_2–ZnO nanocomposite, a standard memory device of thermally annealed ZnO NRs (without adding CeO_2 QDs) was also fabricated, for comparison. Although the I–V behavior of the ZnO NRs exhibited a memory effect (Figure 3a) but the abrupt current transition was not observed, and the memory window

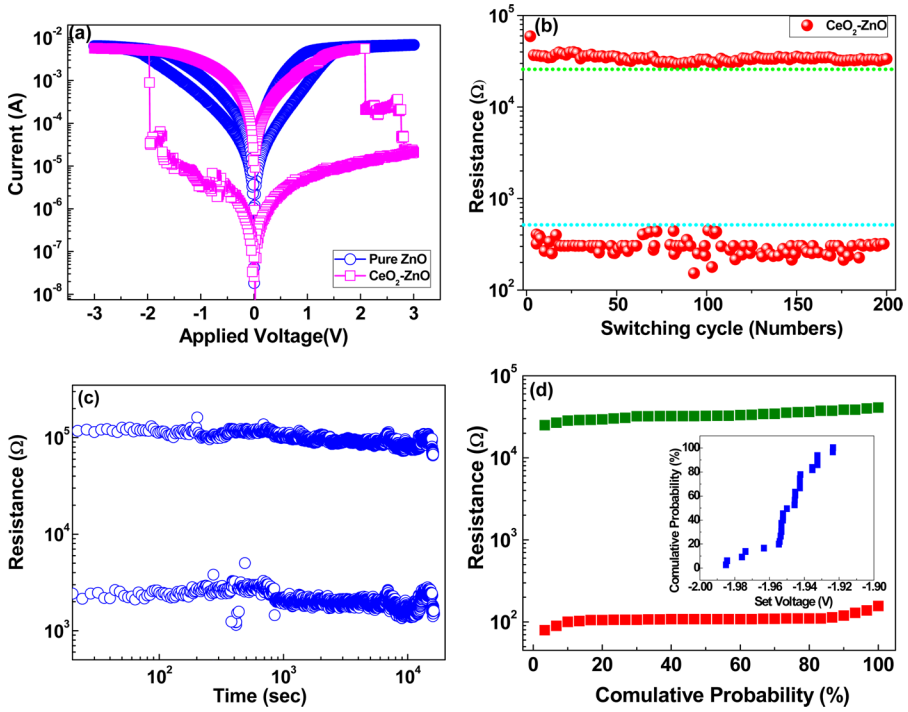

Figure 3. (a) Current–voltage (I–V) characteristics. (b) Endurance cycles characteristics for 60 s. (c) Retention data of HRS and LRS after the RESET and SET, respectively. (d) Statistical distributions of the HRS and LRS (inset shows the distribution of set voltage) of the Au/CeO_2–ZnO/FTO memory device.

dx.doi.org/10.1021/am400168m | ACS Appl. Mater. Interfaces 2013, 5, 2249–2254

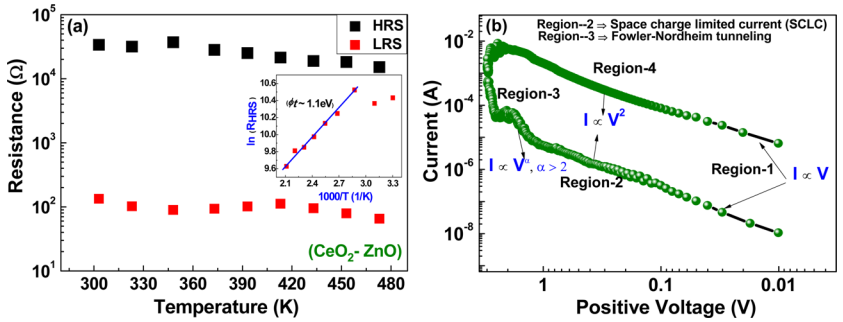

Figure 4. (a) Temperature dependence of R_{OFF} and R_{ON} of the device, implying a semiconducting character. (The inset shows the Arrhenius plot for the OFF state.) (b) Plot of log I vs log V under positive bias, fitted for the trap-controlled space-charge-limited current (SCLC) mechanism for the Au/CeO_2−ZnO/FTO nanocomposite device.

was much smaller than the ZnO−CeO_2 nanocomposite (see Figure S2 in the Supporting Information). This implies that the improvement of RS performance in the CeO_2−ZnO nanocomposite is strongly correlated to the presence of CeO_2 QDs. We also perform the same measurements on CeO_2 QDs layer-by-layer (LBL) assembly without ZnO NRs (results not shown) and found that the reliability is a problem in these devices.

Figure 3d presents the distributions of resistance values in both states (switching threshold voltages (V_{SET}); see the inset) of the device for 30 repeatable switching cycles. The narrow dispersion of switching parameters from their average values indicates high uniformity in the device performance.

We further studied the temperature (T)-dependent resistance (R) of the devices in ON and OFF states in the temperature range of 290−480 K (Figure 4a) (the same measurements for ZnO NRs without CeO_2 QDs were presented in Figure S3 in the Supporting Information). It can be observed that the resistances of HRS and LRS decrease as the temperature increased, implying a semiconductor behavior rather than a metallic one. Therefore, we can rule out the formation and rupture of conductive metallic nanofilaments accounting for the resistive switching behavior in the CeO_2−ZnO nanocomposite. Furthermore, the thermal activation energy (ϕ) was determined to be 1.1 eV via an Arrhenius plot, using the relationship

$$R = R_0 \exp\left(\frac{\phi_t}{kT}\right)$$

where k is the Boltzmann constant, which matches well with the thermal activation energy of 0.8 eV for CeO_2.[17]

Several different mechanisms, such as intermediate-state enhanced tunnelling transport,[18] the trap-filled process affected by space-charge-limited current (SCLC) transport,[19] and the filamentary path mechanism,[20] have been used to explain the switching transition behaviors (current transition) in metal oxide thin films. To investigate the origin of switching mechanism of the CeO_2−ZnO nanocomposite device, the I−V characteristics depicted in a log I vs log V curve are plotted in Figure 4b.

According to this model, free carriers can be thermally generated at low voltage, so linear voltage dependence can be observed (region 1), e.g., $I \propto V$ for Ohmic conduction. By applying a higher applied electric field, these carriers can penetrate into the dielectric/insulating material from a thermionic process across the barrier. As a result, concentration of free carriers (n) is much lower than the trapped charge concentration (n_t). The current−voltage sweep then presents a V^2 dependence, as Mott's V^2 law.[21]

$$J = \frac{9}{8}\varepsilon_0\varepsilon_r\mu\left(\frac{V^2}{L^3}\right)$$

where J is the transport current, ε_r and ε_0 are static dielectric constant and permittivity of free space, μ is the free carrier mobility, V is the applied voltage, and L is the insulator/dielectric layer (thin film) thickness.

For the CeO_2−ZnO nanocomposite, the defects on the CeO_2 QD surface, such as cation or anion dangling bonds, make broad electronic states near the band edge. They serve as hole or electron trappings, which may act as acceptors for carriers. Thus, the concept of shallow traps can be utilized to modify the SCLC model.[22] Since the injected charge carriers can be trapped in the shallow traps, the concentration of the injected charge carriers that freely contribute to the SCLC is reduced by the factor ξ, and the ratio of the total density of free electrons (n) to the trapped electrons (n_t) is given by

$$\xi = \frac{n}{n + n_t}$$

With further increases in applied voltage, Fowler−Nordeim tunnelling may also occur, in addition to the thermionic emission, where the injected free carriers (n) increased rapidly and the traps are nearly filled. The current−voltage sweep showed exponential behavior as $\ln I/V^2 \propto V^{-1}$. At the final stage with the highest applied voltage, the traps are almost filled; the I−V characteristics follow the trap-filled model with I−V^2 dependence.

In the CeO_2−ZnO nanocomposite, each CeO_2 QD may act as a quantum well whose energy levels are not continuous but discrete, thus possess quasi-bound states. The activation energy of these states can be estimated as 1.1 eV, as shown in Figure 4a.

The electrons may probably have chance to be trapped in the QD and, consequently, can block the path to tunnel through during reverse sweep, which results in the OFF state. For negative applied voltage, the electrons continue to fill the charge traps up to highest level (CeO_2 QD may continue to store the charges), which ultimately leads to switch resistance from the HRS state to the LRS state; the entire process is demonstrated schematically in Figure 5. Thus, the QD can act as a capacitor, whose capacitance can be varied in both the regions of HRS and LRS.

The density of charge traps/acceptors is expected to be quite low in ZnO, as compared to CeO_2 (QDs) and the CeO_2−ZnO

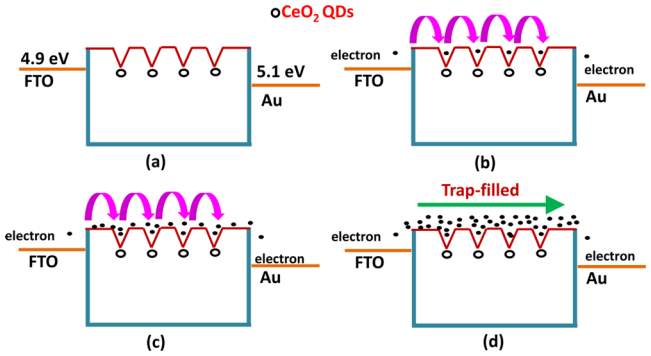

Figure 5. Schematic diagrams for the transport mechanism of trapped-filled space-charge limitation conduction: (a) thermally generated carrier conduction, (b) near empty traps, (c) traps partially filled, and (d) fully filled traps.

nanocomposite. Hence, no significant charge trapping/detrapping effect was expected in ZnO (NRs) array. As a result, no prominent resistive switching effect was observed in this device. For CeO_2 QD-based devices (without ZnO (NRs) matrix), shallow charge traps exist randomly within the matrix of CeO_2 QDs causes poor stability in resistive switching properties. The greater stability and reliability in resistive switching properties of the CeO_2–ZnO nanocomposite can be attributed to the formation of well-aligned shallow traps along and on the surface of the ZnO NRs. The electronic contribution in CeO_2 (charge injection/extraction and accumulation) could be important in the device switching properties. The charge carriers near the interface could be accumulated and depleted during the application of positive and negative electric pulses. Also, the adsorption of CeO_2 QDs on the ZnO NR surface may cause alteration in its electronic band structure and can easily generate surface band bending effect.[23] This surface band bending effect may be more pronounced for 15 layers of CeO_2 QD layers, resulting in reduced conductivity (high resistance change).

It is known that, for nanostructured semiconductors, the surface states play an important role in determining carrier concentration, mobility, and barrier height. Such a heterojunction (CeO_2–ZnO) leads to passivation of surface oxygen by reducing oxygen defects (vacancies) in the ZnO nanorods, which is also consistent to our XPS results (Zn-rich NR surface) (Figure S4 in the Supporting Information). The reduction of the oxygen vacancies further leads to a lowering of the surface barrier, which, in turn, is expected to increase carrier mobility and conductivity. Also, the work function of CeO_2 (4.69 eV), being smaller than that of ZnO (5.3 eV), enables the transfer of electrons from CeO_2 nanoparticles to ZnO, giving rise to a higher carrier concentration in the NRs (energy band diagram schematically depicted in Figure S5 in the Supporting Information). In a recent study, Warule et al. presented a significant reduction in turn on field (off set) strength (~1.8 V/μm) for the nanocomposite structure composed of ZnO nanorods and CeO_2 nanoparticles over other nanostructures.[24]

To further examine the gold top electrode effect, we prepared more than 10 samples (without a gold top electrode) for the measurement. The restive switching behavior was similar to the aforementioned device (with Au top electrode), as shown in Figure S6 in the Supporting Information. Also, to exclude the possible role of the FTO electrode, we also used bare FTO substrate without ZnO NRs and CeO_2 QDs, and a short circuit was clearly observed. Hence, we can confirm that the resistive switching phenomenon is attributed to ZnO–CeO_2 nanocomposites, not from the gold top electrode or the FTO substrate. Besides, the concentration of CeO_2 QDs and their effect on RS properties were also studied. Two samples with different CeO_2 QD layers (5 and 30) were also prepared and found to exhibit RS effect (Figure S7 in the Supporting Information).

The ratios of high resistance state (HRS) to low resistance state (LRS) in these devices were ~8 and ~6.5, respectively, as shown in Figure 6 (the same behavior in linear scale was shown

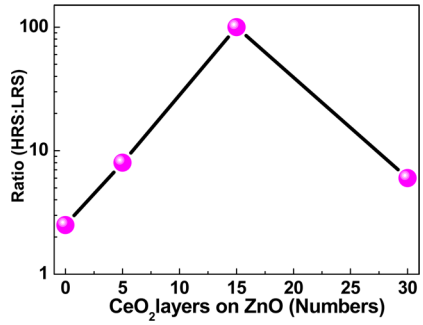

Figure 6. Ratios of high resistance state to low resistance state (HRS:LRS) for different numbers of CeO_2 QD layers on a ZnO NR matrix (in logarithmic scale).

in Figure S8 in the Supporting Information). The different amounts of CeO_2 (QDs) may result different surface conditions, and the spatial distribution of defects may also vary among the samples. The presence of charges may not be sufficient to demonstrate a prominent RS effect for the device embedded with 5 layers of CeO_2 (QDs). For the device with 30 CeO_2 (QDs) layers, CeO_2 QDs might also form a thick/loose layer on the ZnO NR surface, which may cause a change in surface energy/surface geometry, and, thus, ZnO cannot act as effective traps filaments, which could not exhibit such a high HRS:LRS ratio.

CONCLUSION

In summary, we have successfully fabricated a CeO_2 quantum dot (QD)–ZnO nanorod (NR) nanocomposite structure by combining electrochemical deposition, hydrothermal, and dip coating processes. An ON/OFF ratio of more than 10^2, more than 10^2 endurance cycles, retention times of longer than 10^4 s, and high uniformity were achieved in the CeO_2–ZnO nanocomposite device. The resistive switching behavior was explained on the basis of a trap-filled space-charge-limited current (SCLC) mechanism. Furthermore, temperature dependence switching behavior of CeO_2–ZnO nanocomposites and ZnO NRs were studied. Moreover, the gold top electrode effect and CeO_2 (QDs) concentration incorporated on the ZnO NR matrix were investigated to verify the origin of resistive switching properties. The refinement of device structure for the improvement of endurance performance and device response time with speed is underway.

ASSOCIATED CONTENT

Supporting Information

EDX line spectrum of a cross-sectional SEM image of a CeO_2–ZnO nanocomposite, Endurance and temperature dependence measurements for ZnO NRs, XPS, energy band diagram, *I*–*V*

dx.doi.org/10.1021/am400168m | ACS Appl. Mater. Interfaces 2013, 5, 2249–2254

curves of CeO_2−ZnO nanocomposite without (Au) top electrode, RS characteristics of devices with 5 and 30 layers of CeO_2 QDs on ZnO NRs, and HRS/LRS vs number of CeO_2QDs layers on ZnO NRs in linear scale. This information is available free of charge via the Internet at http://pubs.acs.org/.

AUTHOR INFORMATION

Corresponding Author

*Tel.: +61 (0)2 9385 9934. Fax: +61 (0)2 9385 6565. E-mail address: D.Chu@unsw.edu.au.

Notes

The authors declare no competing financial interest.

ACKNOWLEDGMENTS

The authors would like to thank Australian Research Council (Project Nos. DP110102391, DP1096769, FT100100956, and DP0988687) for financially supporting this work.

REFERENCES

(1) Yuriy, V.; Pershin, M. D. V. *Adv. Phys.* **2011**, *60*, 145.
(2) Xu, S.; Wang, Z. *Nano Res.* **2011**, *4*, 1013.
(3) Dong, Y.; Yu, G.; McAlpine, M. C.; Lu, W.; Lieber, C. M. *Nano Lett.* **2008**, *8*, 386.
(4) Nagashima, K.; Yanagida, T.; Oka, K.; Kanai, M.; Klamchuen, A.; Kim, J.-S.; Park, B. H.; Kawai, T. *Nano Lett.* **2011**, *11*, 2114.
(5) Nagashima, K.; Yanagida, T.; Oka, K.; Taniguchi, M.; Kawai, T.; Kim, J.-S.; Park, B. H. *Nano Lett.* **2010**, *10*, 1359.
(6) Oka, K.; Yanagida, T.; Nagashima, K.; Kawai, T.; Kim, J.-S.; Park, B. H. *J. Am. Chem. Soc.* **2010**, *132*, 6634.
(7) Oka, K.; Yanagida, T.; Nagashima, K.; Tanaka, H.; Kawai, T. *J. Am. Chem. Soc.* **2009**, *131*, 3434.
(8) Yang, Y.; Zhang, X.; Gao, M.; Zeng, F.; Zhou, W.; Xie, S.; Pan, F. *Nanoscale* **2011**, *3*, 1917.
(9) Yao, J.; Jin, Z.; Zhong, L.; Natelson, D.; Tour, J. M. *ACS Nano* **2009**, *3*, 4122.
(10) Duclere, J. R.; Doggett, B.; Henry, M. O.; McGlynn, E.; Rajendra Kumar, R. T.; Mosnier, J. P.; Perrin, A.; Guilloux-Viry, M. *J. Appl. Phys.* **2007**, *101*, 013509.
(11) Chang, W.-Y.; Lin, C.-A.; He, J.-H.; Wu, T.-B. *Appl. Phys. Lett.* **2010**, *96*, 242109.
(12) Chu, D.; Younis, A.; Li, S. *J. Phys. D: Appl. Phys.* **2012**, *45*, 355306.
(13) Yang, Y. C.; Pan, F.; Liu, Q.; Liu, M.; Zeng, F. *Nano Lett.* **2009**, *9*, 1636.
(14) Younis, A.; Chu, D.; Li, S. *J. Phys. D: Appl. Phys.* **2012**, *45*, 355101.
(15) Chu, D.; Li, S. *New J. Glass Ceramics* **2012**, *2*, 13.
(16) Dang, F.; Kato, K.; Imai, H.; Wada, S.; Haneda, H.; Kuwabara, M. *Cryst. Growth Des.* **2010**, *10*, 4537.
(17) Liang, H.; et al. *J. Mater. Sci.* **2012**, *47*, 299.
(18) Pei, Z.; Su, A. Y. K.; Hwang, H. L.; Hsiao, H. L. *Appl. Phys. Lett.* **2005**, *86*, 063503.
(19) Lampert, M. A.; Peter, M. *Current Injection in Solids*; Academic Press: New York, 1970; p 14.
(20) Efimenko, K.; Rybka, V.; Švorčík, V.; Hnatowicz, V. *Appl. Phys. A: Mater. Sci. Process.* **1998**, *67*, 503.
(21) Leighton, P. A. Electronic Processes in Ionic Crystals (Mott, N. F.; Gurney, R. W.) (Book review). *J. Chem. Educ.* **1941**, *18*, 249.
(22) Rose, A. *Phys. Rev.* **1955**, *97*, 1538.
(23) Ke, J.-J.; Liu, Z.-J.; Kang, C.-F.; Lin, S.-J.; He, J.-H. *Appl. Phys. Lett.* **2011**, *99*, 192106.
(24) Warule, S. S.; et al. *J. Mater. Chem.* **2012**, *22*, 8887.